The topology of homogeneous isotropic turbulence with passive scalar transport

P. L. O'Neill* J. Soria†

(Received 29 October 2004, revised 18 October 2005)

Abstract

Data obtained from direct numerical simulations of isotropic homogeneous turbulence and the diffusion of a scalar with an applied mean gradient is analysed using the topological techniques developed by Chong, Perry and Cantwell [*Physics of Fluids A*, **2**:765-777, 1990]. Simulations were run at two different Taylor–Reynolds numbers and two different Schmidt numbers. Comparing the numerical results obtained, relationships between the scalar characteristics and the topological features of the flow are identified.

*Formerly of the Laboratory for Turbulence Research in Aerospace & Combustion (LTRAC), Monash University, Melbourne Australia; now at School of Mechanical Engineering, The University of Western Australia, Crawley, Western Australia 6009, Australia mailto:poneill@mech.uwa.edu.au

†LTRAC, Monash University, Melbourne Australia

See http://anziamj.austms.org.au/V46/CTAC2004/Onei for this article, Published November 5, 2005. ISSN 1446-8735

Contents

1 Introduction

Transport of scalars by turbulent fluid motion is of fundamental importance in processes such as pollutant formation, mass and heat transfer and chemical reactions. In recent years there has been a push for improved combustion efficiency and decreased pollutant emissions from a range of devices from power plants to jet engines. These devices generally involve turbulent fluid motion, where the turbulence causes the reactants to mix more rapidly. Particularly in cases of relatively rapid chemical reaction, the mixing property is the major factor determining the rate of reaction. Improved methods for predicting and controlling turbulent flows may therefore lead to improved efficiencies and reduced emissions in a variety of devices.

In this study the distribution of a scalar with an imposed mean gradient in homogeneous isotropic turbulence is investigated using direct numerical

simulation (DNS). The computer program used in this study was developed by Crespo [5]. The full Navier–Stokes and scalar equations for incompressible flow are solved, without modeling, on a three-dimensional grid. The scalar transport equation includes a term for the advection of the scalar Θ by the velocity field $\mathbf{u}$, and another term for the diffusion of the scalar by molecular effects involving the molecular diffusivity, κ:

$$\frac{\partial \Theta}{\partial t} + \mathbf{u} \cdot \nabla \Theta = \kappa \nabla^2 \Theta \,. \tag{1}$$

The scalar is transported by fluid motion and diffused by molecular effects with no reciprocal action on the flow dynamics (it is passive). In the case where a constant mean gradient, β, is imposed the scalar consists of a component due to the imposed gradient, plus a fluctuating term:

$$\Theta(x) = \theta(x) + \beta \cdot x \,. \tag{2}$$

The transport equation for the scalar fluctuation, θ, is

$$\frac{\partial \theta}{\partial t} + \mathbf{u} \cdot \nabla \theta = \kappa \nabla^2 \theta - \beta \cdot u_1 \,, \tag{3}$$

where u_1 is the velocity component in the x direction. The Schmidt number Sc of the scalar is the ratio ν/κ (ν is the kinematic viscosity) and corresponds to the Prandtl number when the scalar is temperature.

2 Velocity gradient tensor analysis

One of the reasons that the physics of scalar transport is not well understood is due to the complex topology of the fluid motions and the three-dimensional complexity of the scalar fields. The development of techniques whereby the topology of the fluids motion is classified by the invariants of the velocity gradient tensor, as seen by a non-rotating observer moving at the same velocity

as the fluid at that point [3], makes it possible to determine the topology distribution in various flows using consistent criteria.

The velocity gradient tensor (VGT)

$$A_{ij} = \frac{\partial u_i}{\partial x_j}\,, \tag{4}$$

where u_i is the velocity vector and x_j is the space vector.

The equation $\det(A - \lambda I) = 0$ finds the characteristic equation of A_{ij}:

$$\lambda_i^3 + P_A\lambda_i^2 + Q_A\lambda_i + R_A = 0\,, \tag{5}$$

where λ_i are the eigenvalues of A_{ij}, and the first, second and third tensor invariants are, respectively,

$$P_A = -A_{ii} = -\mathrm{tr}(A)\,, \tag{6}$$

$$Q_A = -\frac{1}{2}A_{ij}A_{ji} = \frac{1}{2}(P_A^2 - \mathrm{tr}(A^2))\,, \tag{7}$$

$$R_A = -\frac{1}{3}A_{ij}A_{jk}A_{ki} = -\det(A)\,. \tag{8}$$

Einstein notation is used in these equations, so repeated indices indicate summation over indices. For incompressible flow $P_A = 0$ from continuity. The discriminant of A_{ij} for incompressible flow is

$$D_A = \frac{27}{4}R_A^2 + Q_A^3\,. \tag{9}$$

The values of Q_A and R_A can be used to define the topology present at a point in the flow field. Figure 1 is taken from [4] and shows the two dimensional (R_A, Q_A) plane and the four recognised flow topologies defined by the values of Q_A and R_A. The tent-like curve corresponds to the equation $D_A = 0$.

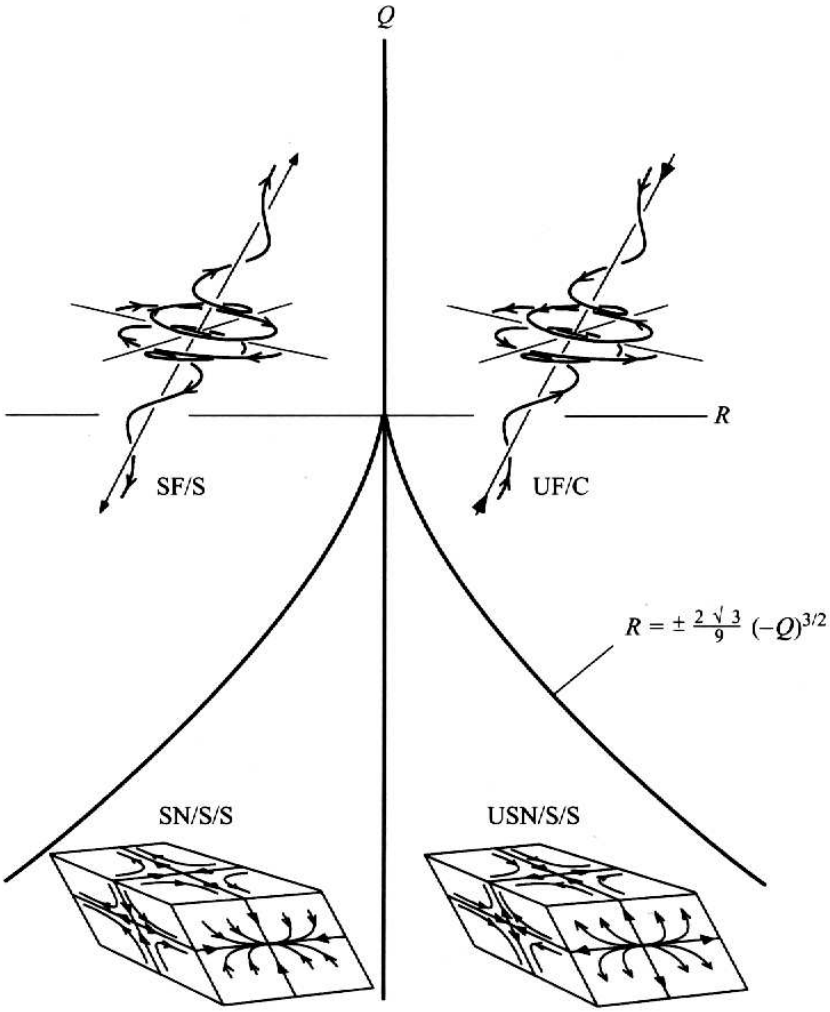

FIGURE 1: Local topologies in the (Q_A,R_A) plane: SF/S, stable focus/stretching; UF/C, unstable focus/contracting; SN/S/S, stable node/saddle/saddle; USN/S/S, unstable node/saddle/saddle.

We decompose the tensor A_{ij} into a symmetric and skew-symmetric part,

$$A_{ij} = S_{ij} + W_{ij}\,, \tag{10}$$

where S_{ij} is the symmetric rate-of-strain tensor and W_{ij} is the skew-symmetric rate-of-rotation tensor:

$$S_{ij} = \frac{1}{2}\left(\frac{\partial u_i}{\partial x_j} + \frac{\partial u_j}{\partial x_i}\right) \quad \text{and} \quad W_{ij} = \frac{1}{2}\left(\frac{\partial u_i}{\partial x_j} - \frac{\partial u_j}{\partial x_i}\right). \tag{11}$$

As with A_{ij}, the tensor S_{ij} has three corresponding invariants (P_S, Q_S and R_S as does W_{ij} (P_W, Q_W and R_W). For incompressible flow $P_S = P_W = P_A = 0$, and $R_W = 0$, and the remaining invariants are

$$Q_S = -\frac{1}{2}S_{ij}S_{ji}\,, \tag{12}$$

$$R_S = -\frac{1}{3}S_{ij}S_{jk}S_{ki}\,, \tag{13}$$

$$Q_W = \frac{1}{2}W_{ij}W_{ij} = \omega_i\omega_i\,. \tag{14}$$

The invariant Q_S measures the local strength of irrotational stretching and is always negative because S_{ij} is a symmetric tensor. The invariant Q_W is proportional to the enstrophy density (the quantity ω_i is a component of the vorticity vector) and is always positive. Note that $Q_A = Q_W + Q_S$.

3 Details of direct numerical simulation

The simulations were carried out on a 128^3 mesh grid with periodicity length of 2π so that the resolved wavenumbers are integral. Table 1 summarises the simulation conditions. The run data are ensemble averages, that is, space and time-averaged quantities. The averaging was undertaken after the simulations had reached a statistically stationary state. Statistical stationarity

Parameter	Tabulated	Run 1	Run 2	Run 3
grid size	N	128	128	128
mean scalar gradient	β	1.0	1.0	1.0
Schmidt number	Sc	0.25	0.25	5.0
kinematic viscosity	ν	0.02	0.007	0.02
Taylor Reynolds Number	Re_λ	42	77	41
largest resolved wave number ($\sqrt{2}N/3$)	$k_{\max}$	60	60	60
smallest resolved length	$1/k_{\max}$	0.0167	0.0167	0.0167
Kolmogorov microscale	η	0.046	0.021	0.046
Corrsin–Oboukhov length scale	η_{CO}	0.122	0.052	
Batchelor microscale	η_{B}			0.021

TABLE 1: Input parameters and run data for the three simulations

of the scalar distribution was typically achieved after $\sim$ 40–50 eddy turnover times, and the scalar field was added into the simulation after the velocity field had attained stationarity. In order to maintain stationarity, the velocity field was forced such that energy production and dissipation were equal. In using the forcing scheme, it was assumed that the small scales do not depend directly on the large scales in the flow.

Included in Table 1 is the Corrsin–Oboukhov length scale and the Batchelor microscale [1]. Theoretical considerations have found that the smallest scalar dissipation scale for the situation where $\mathrm{Sc} < 1$ is the Corrsin–Obukhov length scale, calculated according to $\eta_{\mathrm{CO}} = \mathrm{Sc}^{-3/4}\eta$ (η is the Kolmogorov microscale). For the situation where $\mathrm{Sc} > 1$ the smallest scalar dissipation scale is the Batchelor microscale, calculated according to $\eta_{\mathrm{B}} = \mathrm{Sc}^{-1/2}\eta$. For the situation where $\mathrm{Sc} = 1$, both of these equations reduce to the same solution, that is, $\eta_{\mathrm{CO}} = \eta_{\mathrm{B}} = \eta$

For all the simulations the Kolmogorov microscale and, depending on which is appropriate, the Corrsin–Oboukhov length scale and Batchelor microscale exceed the smallest resolved length of 0.0165. Therefore, the velocity and scalar fields were resolved.

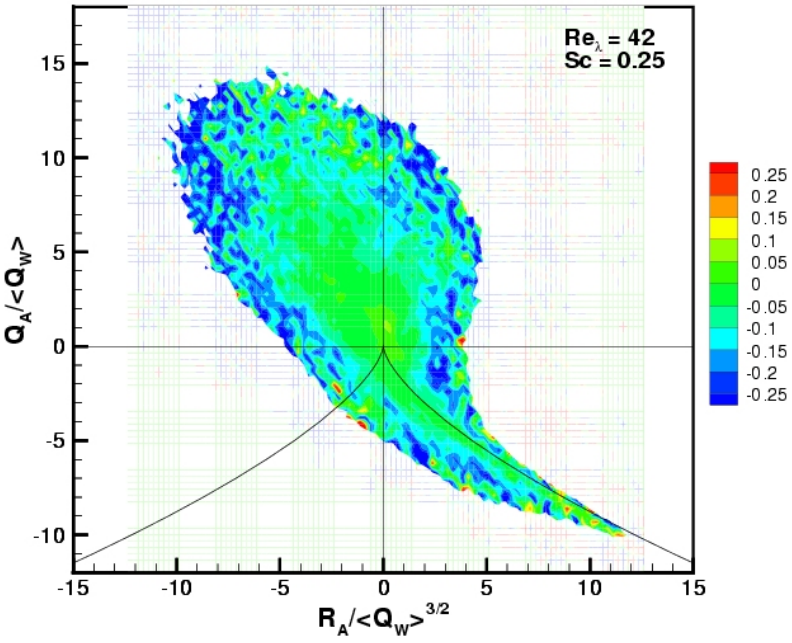

FIGURE 2: Results for $\mathrm{Re}_\lambda = 42$; $\mathrm{Sc} = 0.25$. Distribution of the conditional mean of the scalar fluctuation, scaled by its ensemble standard deviation (the ensemble mean scalar fluctuation is zero), $\theta/\langle s_\theta\rangle$, conditioned on the invariants Q_A and R_A, scaled by $\langle Q_W\rangle$ and $\langle Q_W\rangle^{3/2}$ respectively.

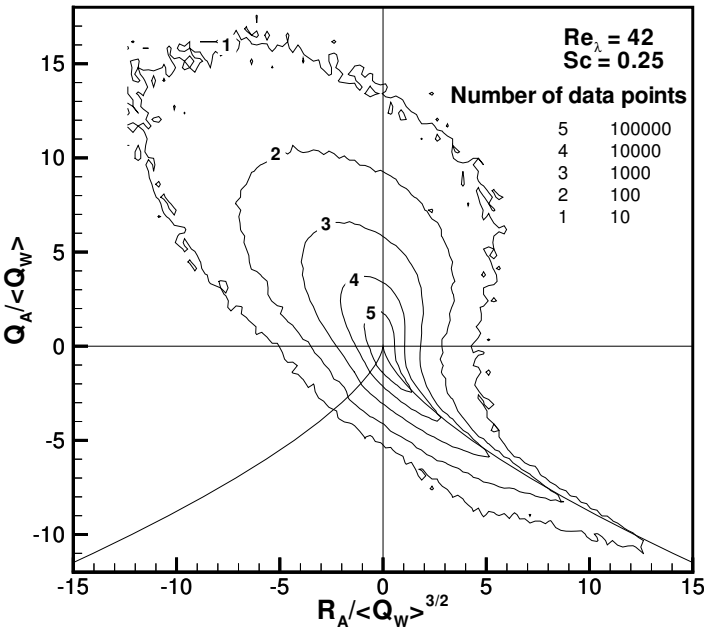

FIGURE 3: Results for $\mathrm{Re}_\lambda = 42$; $\mathrm{Sc} = 0.25$. Contours showing where the fluid elements are located in the (Q_A,R_A) plane.

4 Results and Discussion

4.1 Velocity gradient tensor analysis

4.1.1 Scalar fluctuation and dissipation in the (Q_A,R_A) plane

The relationship between the scalar and the local topology is shown in the conditional mean distribution of Figures 2 and 3, which shows the mean scalar fluctuation, scaled by its standard deviation (the ensemble mean scalar fluctuation is zero), θ/s_θ, and conditioned on the invariants Q_A and R_A, scaled by $\langle Q_W \rangle$ and $\langle Q_W \rangle^{3/2}$ respectively. (Angled brackets indicate ensemble averages.) Figure 4 shows the conditional mean scalar dissipation, scaled by its ensemble mean, $\varepsilon/\langle\varepsilon\rangle$, in the same plane. The data for these plots was obtained by combining the results taken at random intervals during a simulation run over greater than twenty eddy turnover times. Normalising Q_A and R_A by $\langle Q_W \rangle$ and $\langle Q_W^{3/2} \rangle$ allows direct comparison between simulations with different Re_λ. A minimum of 20 data points were available for determination of the conditional mean within each conditional domain.

From Figure 2, it appears that the mean scalar fluctuation is virtually uniform, regardless of local topology, which is consistent with the scalar being well-mixed. Figure 3 shows the distribution in the number of data points across the (Q_A, R_A) plane for Run 1. Most of the data points are located in the region closest to the point $Q_A = R_A = 0$, and the population decreases exponentially away from small Q_A and R_A values. Extreme scalar values are generally located on the edges of the tear-drop shaped region where the number of data points is low. Therefore extreme scalar values may be due to a small number of very large positive or negative values.

Figure 4 shows the distribution of the mean scalar dissipation with topol-

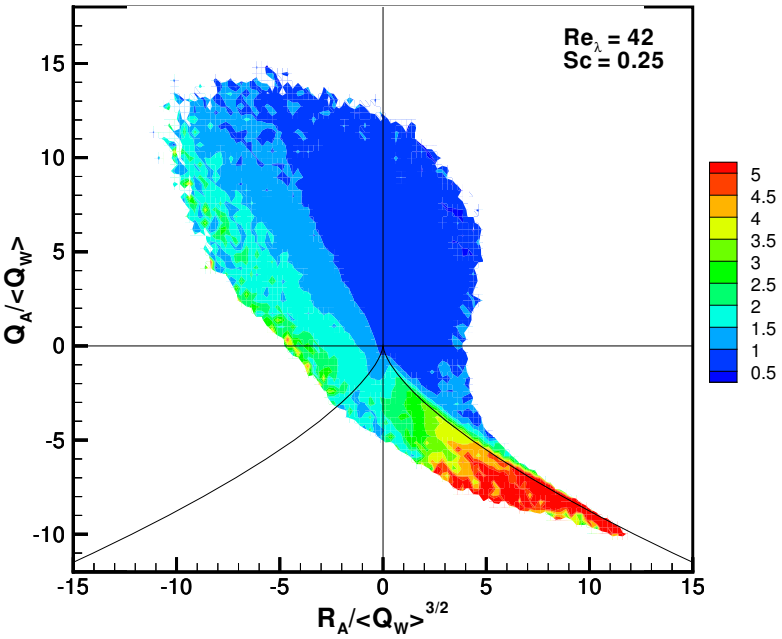

FIGURE 4: Distribution of the conditional mean of the scalar dissipation, scaled by its ensemble mean scalar dissipation, $\varepsilon/\langle\varepsilon\rangle$, conditioned on $Q_A/\langle Q_W\rangle$ and $R_A/\langle Q_W\rangle^{3/2}$. $\mathrm{Re}_\lambda = 42$; $\mathrm{Sc} = 0.25$.

ogy. The dissipation of the scalar fluctuations is calculated by

$$\varepsilon = \kappa \left(\frac{\partial \theta}{\partial x_i} \frac{\partial \theta}{\partial x_i} \right) . \tag{15}$$

From Figure 4 it appears that the highest mean scalar dissipation values are found where R_A is positive, and Q_A and D_A are negative, which, referring to Figure 1, indicates UN/S/S topology. In comparison, the lowest mean scalar dissipation values are located predominantly where R_A, Q_A and D_A are all positive, that is, in regions where the flow is UF/C. Moderate mean scalar dissipation values are found where SN/S/S topologies occur, while moderate to low mean scalar dissipation values occur in regions of SF/S topology. This is consistent with the results of Brethouwer et al. [2], who found a similar distribution for mean scalar gradient conditioned on topology.

4.1.2 Scalar dissipation conditioned on $-Q_S$ and Q_W

In Figures 5 and 6 are shown the mean scalar dissipation conditioned on $-Q_S$ and Q_W. The dependence of mean scalar dissipation on $-Q_S$ appears to be almost linear for low $-Q_S/\langle Q_W \rangle$, with the dependence becoming weaker as $-Q_S/\langle Q_W \rangle$ increases above a certain value. From the data presented it appears that the limit at which the dependence changes is related to the flow conditions. The limit appears to decrease with increasing Re_λ for $\mathrm{Sc} = 0.25$, and decrease with increasing Sc for $\mathrm{Re}_\lambda \sim 42$.

The relationship between the local value of $-Q_S$ and the local scalar dissipation is investigated further by examining the results for $-Q_S$ and θ in a single plane of the simulation volume. Figure 7 compares a single xy plane from each of the simulation volumes with the same Sc but different Re_λ, whereas Figure 8 compares a single xy plane from each of the simulation volumes with the same Re_λ but different Sc.

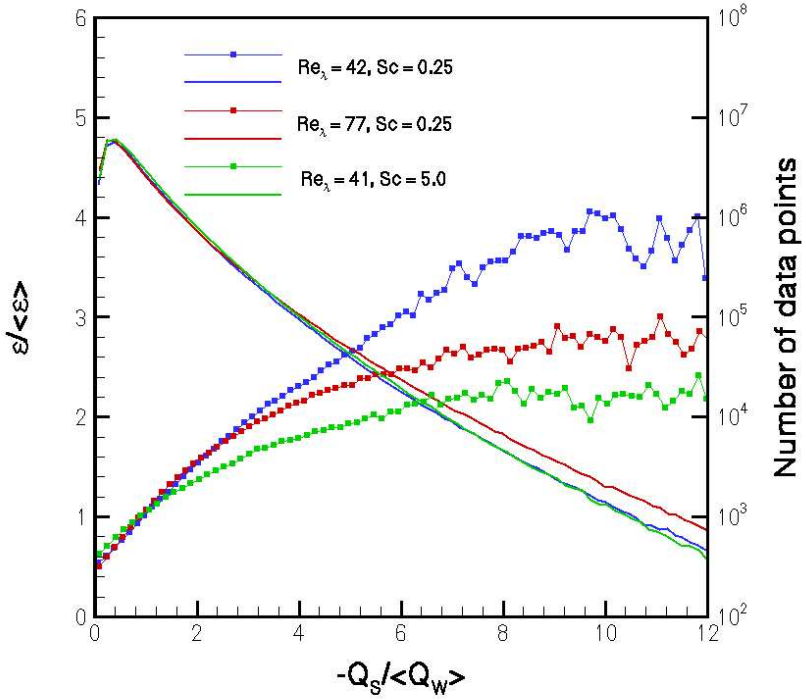

FIGURE 5: Mean scalar dissipation, scaled by its ensemble mean, and conditioned on $-Q_S/\langle Q_W \rangle$.

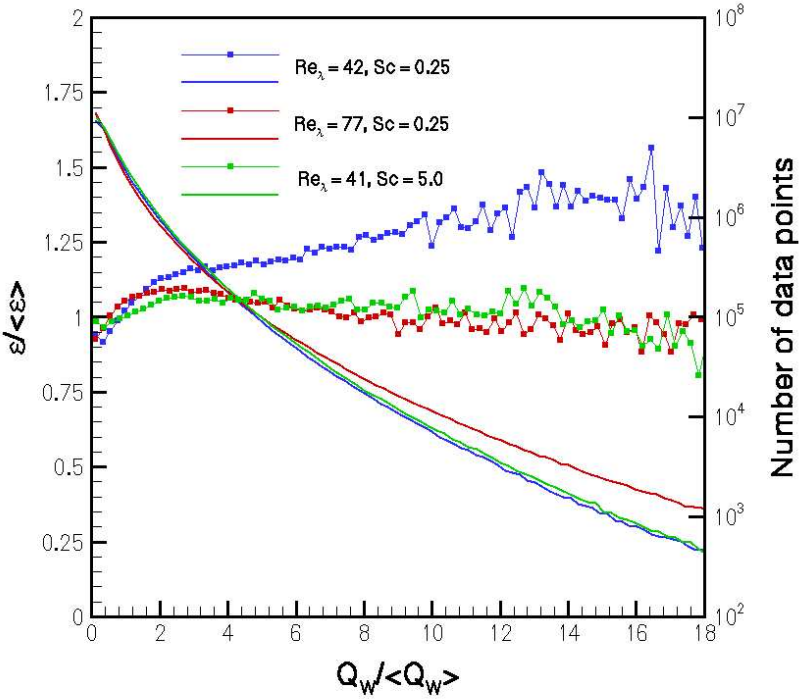

FIGURE 6: Mean scalar dissipation, scaled by its ensemble mean, and conditioned on $Q_W/\langle Q_W \rangle$.

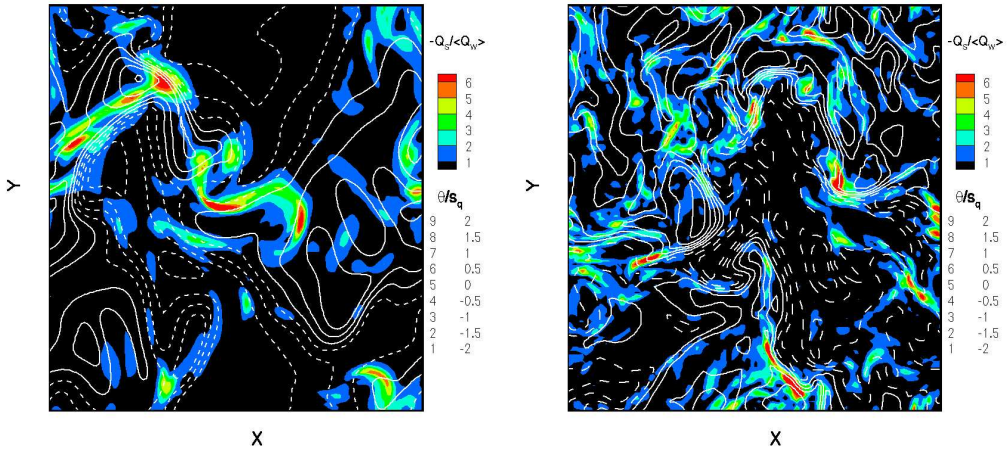

(a) (b)

FIGURE 7: Examples of the 2-dimensional xy plane showing contours of constant scalar fluctuation (θ/s_θ) and $-Q_S/\langle Q_W \rangle$ for a constant Schmidt number ($\mathrm{Sc} = 0.25$) and varying Reynolds number: (a) $\mathrm{Re}_\lambda = 42$; (b) $\mathrm{Re}_\lambda = 77$. The coloured contours are for $-Q_S/\langle Q_W \rangle$. Contour lines of constant θ/s_θ are separated by 0.5: solid line, positive scalar fluctuation; dashed line, negative scalar fluctuation.

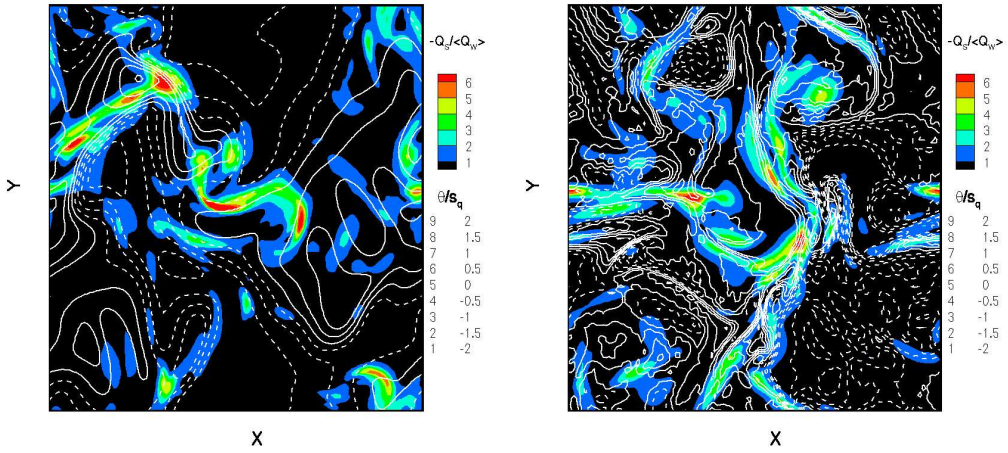

(a) (b)

FIGURE 8: Examples of the 2-dimensional xy plane showing contours of constant scalar fluctuation (θ/s_θ) and $-Q_S/\langle Q_W \rangle$ for a constant Reynolds number ($\mathrm{Re}_\lambda \sim 42$) and varying Schmidt number: (a) $\mathrm{Sc} = 0.25$; Right: (b) $\mathrm{Sc} = 5.0$. The coloured contours are for $-Q_S/\langle Q_W \rangle$. Contour lines of constant θ/s_θ are separated by 0.5: solid line, positive scalar fluctuation; dashed line, negative scalar fluctuation.

From the scalar transport equation (3) see that there is a term that describes the advection of the scalar fluctuation by the velocity, and another term that describes the diffusion of the scalar fluctuation. According to Gibson [6], the velocity term serves to promote scalar fluctuation, whereas the diffusivity term serves to dampen out scalar fluctuations. The differences between the two graphs shown in Figure 7 is attributed to changes in the advection term of the scalar transport equation, which result in a reduction in the size of the approximately isoscalar surfaces, and an increase in the frequency of peaks and troughs in the scalar fluctuation field. The differences between the two graphs shown in Figure 8 is attributed to changes in the diffusion term of the scalar transport equation, which results in a reduction in the size of the approximately isoscalar surfaces, and an increase in the frequency of peaks and troughs in the scalar fluctuation field when the value of κ is decreased.

5 Conclusions

From DNS of homogeneous isotropic turbulence we have compared the velocity and scalar fields obtained for different Reynolds numbers (Re_λ) and Schmidt numbers (Sc). The results confirm the importance of the local rate of strain to the mixing of the scalar. In addition, differences in the velocity and scalar fields are attributed to differences in Sc and Re_λ. Increasing Re_λ or Sc resulted in a decrease in the size of the approximately isoscalar surfaces in the flow and an increase in the frequency of peaks and troughs in the scalar fluctuation field. Although changing Sc and Re_λ had the same effect, the reason for the change in the two cases was different. Increasing Re_λ influenced the velocity term in the scalar transport equation, whereas increasing Sc influenced the diffusion term in the scalar transport equation.

Acknowledgments: The authors gratefully acknowledge the support of the ARC and APAC and VPAC.

References

[1] Arpaci, V. S. Microscales of turbulent combustion. *Progress in Energy and Combustion Science*, **21**(2):153–171, 1995. http://dx.doi.org/10.1016/0360-1285(95)00002-Y C1176

[2] Brethouwer, G., Hunt, J. C. R. and Nieuwstadt, F. T. M. Micro-structure and Lagrangian statistics of the scalar field with a mean gradient in isotropic turbulence. *Journal of Fluid Mechanics*, **474**:193–225, 2003. http://dx.doi.org/10.1017/S0022112002002549 C1181

[3] Chong, M. S., Perry, A. E. and Cantwell, B. J. A general classification of three-dimensional flow fields. *Physics of Fluids A*, **2**(5):765-777, 1990. C1173

[4] Chong, M. S., Soria, J., Perry, A. E., Chacin, J., Cantwell, B. J and Na, Y. Turbulence structure of wall-bounded shear flows found using DNS data. *Journal of Fluid Mechanics*, **357**:225–247, 1998. C1173

[5] Crespo, B. *Simulación numérica directa de escalares inertes y reactivos*, Report from the Departamento de Cienca y Tecnologia de Materiales y Fluidos, Universidad de Zaragoza, 1994 C1172

[6] Gibson, C. H. Fine structure of scalar fields mixed by turbulence. I. Zero-gradient points and minimal gradient surfaces. *Physics of Fluids*, **11**(11):2305–2315, 1968. C1186